Periodic Surface Topology of Three−Arm Semifluorinated Alkane Monodendron Diblock Copolymers

ARTICLE *in* LANGMUIR · JULY 2001

Impact Factor: 4.46 · DOI: 10.1021/la010510m

8 AUTHORS, INCLUDING:

Easan Sivaniah
University of Cambridge
62 PUBLICATIONS **1,077** CITATIONS

SEE PROFILE

Glenn H Fredrickson
University of California, Santa Barbara
434 PUBLICATIONS **28,398** CITATIONS

SEE PROFILE

Christopher K Ober
Cornell University
587 PUBLICATIONS **15,869** CITATIONS

SEE PROFILE

Periodic Surface Topology of Three-Arm Semifluorinated Alkane Monodendron Diblock Copolymers

E. Sivaniah,† J. Genzer,‡ G. H. Fredrickson, and E. J. Kramer*

Departments of Materials and Chemical Engineering, University of California Santa Barbara, Santa Barbara, California 93106-5050

M. Xiang, X. Li, and C. Ober

Department of Materials Science and Engineering, Cornell University, Ithaca, New York 14853-1501

S. Magonov

Digital Instruments, Santa Barbara, California 93106

Received April 5, 2001. In Final Form: April 16, 2001

Scanning force microscopy has been used to reveal the surface topology of the smectic B phase of (styrene−isoprene) diblock copolymers that have semifluorinated (SF) alkane mesogens attached as three-arm monodendrons to the isoprene backbone. On the largest length scales, the block copolymers microphase separate into well-known diblock copolymer microstructures and evidence of these can been seen in the surface topology. However, there are periodic surface structures, so-called domes (with periodicities of about 18.5 nm), that arise solely from the arrangement of the SF mesogens at the polymer surface. These domes are intrinsically independent of the much larger morphology of the block copolymer. Very long range (ca. micrometers) ordering of the domes is possible for lamellar block copolymer microstructures if the surfaces are prepared by very slow cooling from the isotropic to the smectic B phase. We infer that the domes arise because of spontaneous surface curvature resulting from mesogen crowding within the monodendrons.

1. Introduction

Coil−coil A−B block copolymers that incorporate a liquid crystalline character within the microstructure have recently attracted considerable interest. Such block copolymers have been synthesized by several ingenious methods that allow side chain mesogenic groups to be attached to a polymer backbone.[1−5] The addition of a liquid crystalline (LC) character to one of the blocks means that there is the potential for structural organization on several length scales. On the largest length scale, there is the domain structure that results from ordering of the block copolymer.[6] The side chain mesogens will change the persistence length of the modified block and thus have an effect on this microphase-separating length scale. However, these changes are small compared to those seen for block copolymers containing rigid rod mesogenic blocks, the so-called rod−coil block polymers.[7]

Within the LC domains of the microphase-separated structure, the mesogens can organize into smectic or other liquid crystalline microstructures characterized by a second length scale. Of particular interest has been how the two structures (LC and microphase) affect one another. For example, it has been shown for the smectic type LC mesophases that the smectic layers are generally formed perpendicular to the microphase interfaces in the bulk block copolymer.[8−12]

Control of mesogenic organization at the surfaces of side chain liquid crystalline polymer films is interesting from both a technological and fundamental perspective. Such films have potential applications ranging from optical switching devices to low surface energy coatings. By analogy to previous studies of amorphous block copolymers and small molecule liquid crystals, questions are now asked about the role of the substrate and surface on both microphase and mesogen organization. Techniques such as scanning force microscopy (SFM), transmission electron microscopy (TEM), X-ray reflectometry,[13,14] and near edge X-ray absorption fine structure (NEXAFS)[15] have been used to reveal the structure of such films. For LC side chain homopolymers, it has been shown that homeotropic

* To whom correspondence should be addressed.
† Present address: Dept. of Polymer Chemistry, Kyoto University, Kyoto 606-8501 Japan.
‡ Present address: Dept. of Chemical Engineering, North Carolina State University, Raleigh, North Carolina 27695−7905.

(1) Adams, J.; Gronski, W. *Makromol. Chem., Rapid Commun.* **1989**, *10*, 553−557.
(2) Fischer, H.; Poser, S.; Arnold, M. *Macromolecules* **1995**, *28*, 6957−6962.
(3) Ruokolainen, J.; Makinen, R.; Torkkeli, M.; Makela, T.; Serimaa, R.; Brinke, G. T.; Ikkala, O. *Science* **1998**, *280*, 557−560.
(4) Stewart, D.; Imrie, C. T. *Macromolecules* **1997**, *30*, 877−884.
(5) Ujiie, S.; Iimura, K. *Macromolecules* **1992**, *25*, 3174−3178.
(6) Bates, F. S.; Fredrickson, G. H. *Annu. Rev. Phys. Chem.* **1990**, *41*, 525.
(7) Chen, J. T.; Thomas, E. L.; Ober, C. K.; Mao, G. P. *Science* **1996**, *273*, 343−346.
(8) Fischer, H.; Poser, S.; Arnold, M. *Liq. Cryst.* **1995**, *18*, 503−509.
(9) Mao, G. P.; Wang, J. G.; Clingman, S. R.; Ober, C. K.; Chen, J. T.; Thomas, E. L. *Macromolecules* **1997**, *30*, 2556−2567.
(10) Sentenac, D.; Demirel, A. L.; Lub, J.; de Jeu, W. H. *Macromolecules* **1999**, *32*, 3235−3240.
(11) Wang, J. G.; Mao, G. P.; Ober, C. K.; Kramer, E. J. *Macromolecules* **1997**, *30*, 1906−1914.
(12) Wu, J. S.; Fasolka, M. J.; Hammond, P. T. *Macromolecules* **2000**, *33*, 1108.
(13) Wong, G. C. L.; Commandeur, J.; Fischer, H.; de Jeu, W. H. *Phys. Rev. Lett.* **1996**, *77*, 5221−5224.
(14) Henn, G.; Stamm, M.; Poths, H.; Rucker, M.; Rabe, J. P. *Physica B* **1996**, *221*, 174−184.
(15) Genzer, J.; Sivaniah, E.; Kramer, E. J.; Wang, J.; Körner, H.; Ober, C. K.; Char, K.; DeKoven, B. M.; Bubeck, R. A.; Fischer, D. A.; Sambasivan, S. *Langmuir* **2000**, *16*, 1993−1997.

10.1021/la010510m CCC: $20.00
Published on Web 06/16/2001

Table 1. Chemical Makeup, Dome Periodicities, and Smectic Transitions of Modified Block Copolymers Studied

sample ID	backbone composition PS/PI mol wt (before attachment)	attachment ratio	*f* value	PS/PILC mol wt (after attachment)	λ_c (nm)	S_B−I temp (°C)
$BC_{0.26}$-$3A_{0.53}$F8H10	38.2K/6.7K	0.531	0.26	38.2K/107.1K	19.4	62.4
$BC_{0.25}$-$3A_{0.58}$F8H10	38.2K/6.7K	0.585	0.25	38.2K/114.9K	17.7	63.6
$BC_{0.21}$-$3A_{0.73}$F8H10	38.2K/6.7K	0.733	0.21	38.2K/141.9K	18.3	64.2
$BC_{0.42}$-$3A_{0.56}$F8H10	66.0K/5.5K	0.562	0.42	66.0K/90.9K	19.3	63.3
$BC_{0.54}$-$3A_{0.58}$F8H10	117K/5.9K	0.587	0.54	117K/101.6K	17.9	64.6
$BC_{0.72}$-$3A_{0.42}$F8H10	215K/6.3K	0.420	0.72	215K/79.9K	18.1	63.9

smectic layers form as a result of strong mesogenic anchoring to a substrate.[16] Moreover, the polarity of the side chain terminal groups will influence the extent to which homeotropic surface organization is seen. The surface organization (e.g., orientation order parameter) shows changes with temperature that roughly mirror those observed for the bulk as the film is heated into the isotropic regime. However, a residual orientation order in the surface layer well above the bulk smectic to isotropic transition temperature suggests a strong ordering influence of the planar surface.[15]

The thickness of a thin film generally provides an extra parameter to manipulate structure. A film thickness incommensurate with the thickness of an integral number of smectic layers can lead to terracing of the smectic layers at the polymer surface. This is analogous to the island (or hole) structure observed for symmetric block copolymer thin films.[13,17,18] These considerations suggest that the interplay between the smectic organization and the larger microphase block copolymer microstructure of thin films of smectic LC side chain block copolymers could prove quite interesting.

In this paper, we consider the surface organization and structure in thin films of block copolymers that have been modified by the addition of semifluorinated three-arm monodendron mesogen side chains. Such polymers were primarily synthesized for their potential to form a stable, low surface energy, smectic B surface layer that is resistant to reconstruction in an aqueous environment.[11] Homopolymers with different, more bulky monodendron side chains have been investigated previously.[19−21] These studies, generally devoted to the bulk properties of the materials, have shown that first generation flat-tapered and second generation conical monodendrons self-assemble into supermolecular cylindrical and spherical dendritic structures. In this paper, we study polymers with much smaller semifluorinated three-arm monodendritic mesogen side chains. We show that these side chains organize into smectic liquid crystal structures in the bulk and produce unique surface topologies that we believe are a direct result of the inability of the dendritic mesogens to pack efficiently at a planar surface.

2. Experimental Section

Block copolymers with semifluorinated monodendron side groups were synthesized by attachment of a first generation three-armed monodendron acid chloride to a hydroxylated poly(styrene-*b*-1,2/3,4-isoprene) (PS-*b*-PI). Each monodendron arm contained the structure $-(CH_2)_{10}-(CF_2)_8F$. A typical attachment is shown schematically in Figure 1. A convergent growth strategy was developed to synthesize the monodendron groups in good yield using an approach that could be extended to higher generation monodendrons. High extents of attachment were achieved despite the steric effects of the bulky monodendron side groups.[22] By anionic polymerization of the precursor PS-*b*-PI backbone and by variation of the extent of attachment of the three-arm monodendron mesogens to the PI block, it was possible to synthesize polymers with volume fractions *f* of polystyrene in the block copolymer ranging from 0.21 to 0.73. These samples, whose parameters are shown in Table 1, are labeled as BC_f-$3A_y$F8H10, where *y* indicates the fraction of isoprene repeat units that possess an attached three-armed mesogen.

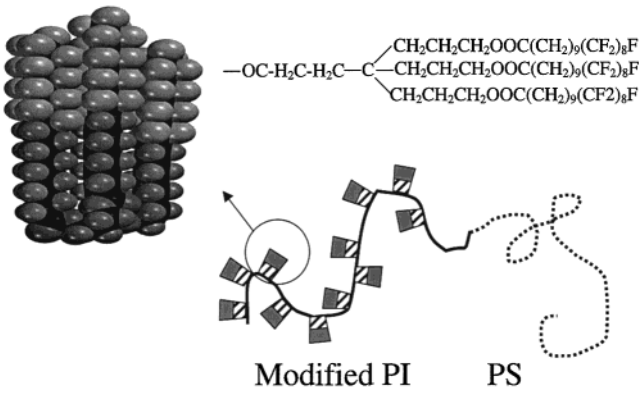

Figure 1. The three-arm monodendron side chain attachment to the PI−PS backbone is shown with a 3D rendering of the mesogen structure. The lighter and darker colored regions refer to the $-CF_2-$ and $-CH_2-$ blocks, respectively. The chemical structure of the monodendron is also given.

Aspects of the surface and bulk structure, morphology, and thermal behavior of these polymers were studied by a combination of analytical techniques including TEM, NEXAFS, and differential scanning calorimetry (DSC). Pertinently, NEXAFS reveals that the surface at room temperature consists entirely of semifluorinated mesogens that are oriented (but with modest orientation order).[22] DSC, supplemented by X-ray diffraction, has revealed there is a single smectic B (S_B) to isotropic (I) bulk transition temperature for these polymers at ∼60 °C (see Table 1).[22] In this paper, we are particularly interested in the surface topology of the films at room temperature.

Samples were prepared by spin-casting solutions of the polymers in α-α-α-trifluorotoluene. Films of thickness ∼150−300 nm were then annealed at 150 °C in ultrahigh vacuum (10^{-8} Torr) and cooled to room temperature at two extreme cooling rates. The first involved rapidly quenching the sample temperature to room temperature (∼100°/min). The second involved a very slow cooling rate (∼0.2°/min). The films were subsequently analyzed with tapping mode scanning force microscopy (TMSFM). Typical operation parameters were as follows: All scans were operated in the repulsive regime of the tip−sample interaction and under "light" tapping conditions, where the ratio of the contact set point amplitude to the free oscillation amplitude was ∼0.75. A cantilever with an etched silicon tip (with a natural frequency of ∼160 Hz) and a multimode SFM (Digital Instruments) were employed for all the SFM data collected.

(16) Jerome, B.; Commandeur, J.; de Jeu, W. H. *Liq. Cryst.* **1997**, *22*, 685−692.
(17) Sheiko, S.; Lermann, E.; Moller, M. *Langmuir* **1996**, *12*, 4015.
(18) Wielen, M. W. J. v. d.; Cohen-Stuart, M. A.; Fleer, G. J. *Langmuir* **1997**, *13*, 4762−4766.
(19) Percec, V.; Ahn, C. H.; Ungar, G.; Yeardley, D. J. P.; Moller, M.; Sheiko, S. S. *Nature* **1998**, *391*, 161−164.
(20) Hudson, S. D.; Jung, H. T.; Percec, V.; Cho, W. D.; Johansson, G.; Ungar, G.; Balagurusamy, V. S. K. *Science* **1997**, *278*, 449−452.
(21) Prokhorova, S. A.; Sheiko, S. S.; Ahn, C. H.; Percec, V.; Moller, M. *Macromolecules* **1999**, *32*, 2653−2660.
(22) Xiang, M.; Li, X.; Ober, C. K.; Char, K.; Genzer, J.; Sivaniah, E.; Kramer, E. J.; Fischer, D. A. *Macromolecules* **2000**, *33*, 6106−6119.

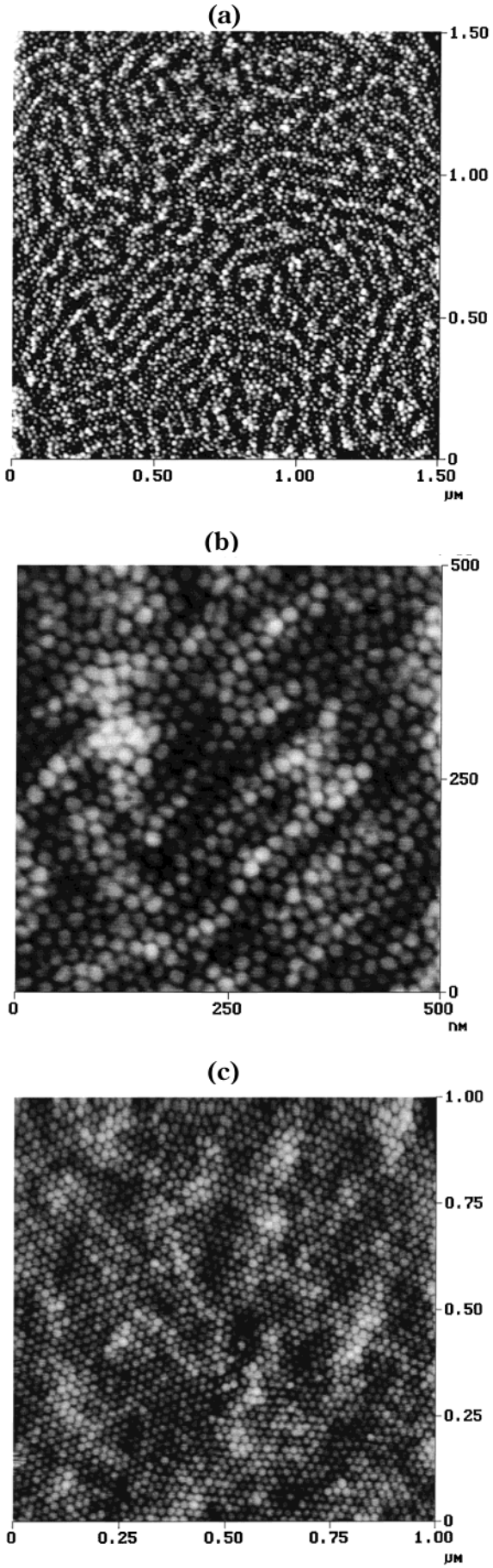

Figure 2. SFM images of $BC_{0.26}$-$3A_{0.53}$F8H10 at (a) low resolution and (b) high resolution and (c) $BC_{0.54}$-$3A_{0.58}$F8H10 at low resolution. The height scale is 10 nm.

3. Results

Three characteristic SFM images are given in Figure 2. Figure 2a shows the large-scale height SFM data for the sample $BC_{0.26}$-$3A_{0.53}$F8H10. In the bulk, this sample, as expected from its *f* value, produces a cylindrical domain structure. The SFM image reveals the large-scale structure of microphase-separated PS cylinders (within a PI matrix) lying parallel to the substrate. This cylindrical morphology is observed in the light tapping mode, indicating that it is a real topological feature. Ideally, however, surface tension effects should lead to macroscopically flat films. We believe that the observed topology arises from the differences in expansion coefficient of the PS and LC monodendron PI (LCMPI) blocks. PS is a glass at room temperature, whereas LCMPI remains relatively elastomeric. This aspect of the SFM images is lost as the polymer microphase separation structures become lamellar because differential contraction of the lamellae will primarily take place perpendicular to the polymer surface. Lateral buckling will be constrained by the glassy PS lamellae. At large *f* values, the majority domain is polystyrene, which vitrifies first producing a matrix that is unyielding to the subsequent contraction effects of the PI blocks. Thus, the presence of the cylindrical morphology does not become manifest at the polymer surface of high *f* value copolymers. Although such surface features in the unmodified block copolymer have been reported before, it is not generally clear whether the observed features were truly topographical or whether they were due to a differential deformation of the polymer surface by the probe tip.[23]

However, the remarkable aspect of Figure 2a is the obvious surface substructure of regular domes that occurs at a smaller length scale than that of the block copolymer. This is shown in greater detail (for sample $BC_{0.26}$-$3A_{0.53}$-F8H10) in Figure 2b. All the block copolymers with this monodendron attachment were found to have these small-scale structures, that we call domes, whereas similar experiments on block copolymers modified with non-monodendron semifluorinated F8H10 mesogens show no surface domes. Moreover, the degree of organization and monodispersity of the size of these domes is related to the rate at which the samples were cooled to room temperature. A more quantitative analysis of the dome structures was obtained by Fourier analysis of the SFM data. In this analysis, which was available via Digital Instruments software, the inverse length scale, $1/\lambda$, was calculated from the wavenumber and the lateral size of the SFM scan. The resulting azimuthally averaged power spectral densities (PSD) obtained for samples cooled at two extremely different rates clearly indicate that the achievement of long-range order is a kinetically controlled process (Figure 3). At slow cooling rates, it is possible to obtain a much more uniform arrangement of the domes. The surface of the *lamellar* block copolymer $BC_{0.54}$-$3A_{0.58}$F8H10 shows *hexagonally* ordered domes with quite long range order after slow cooling as seen in Figure 2c.

The average center-to-center distance, λ_c, and a measure of the long-range order of the domes can be extracted from the position and width of a Gaussian fit to the PSD. Moreover, a series of SFM line scans can be used to evaluate the average amplitude, *a*, of the domes. The characteristic periodicity λ_c (18.5 ± 1 nm) was remarkably constant for all the polymers studied in this paper (see Table 1).

The line scan analysis showed that $a = 1.00 \pm 0.27$ nm. The broad distribution in *a* was due in part to the fact

(23) Magonov, S. N.; Elings, V.; Whangbo, M.-H. *Surf. Sci.* **1997**, *375*, L385.

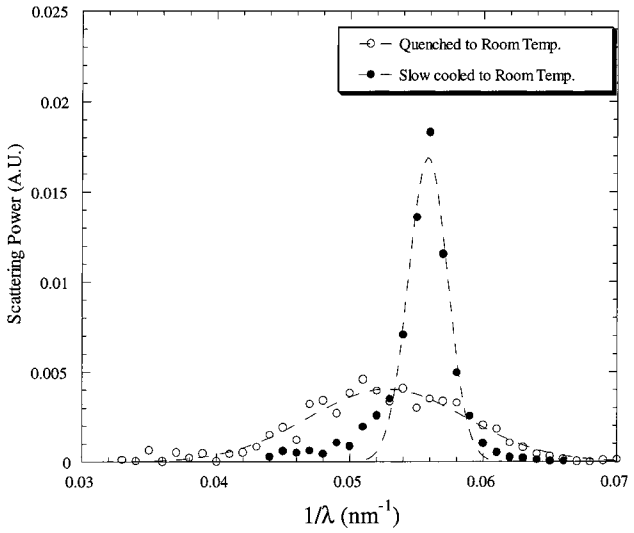

Figure 3. The 2D averaged power spectral density of sample $BC_{0.54}$-$3A_{0.58}$F8H10 under two extreme annealing histories. (Lines shown are Gaussian fits.)

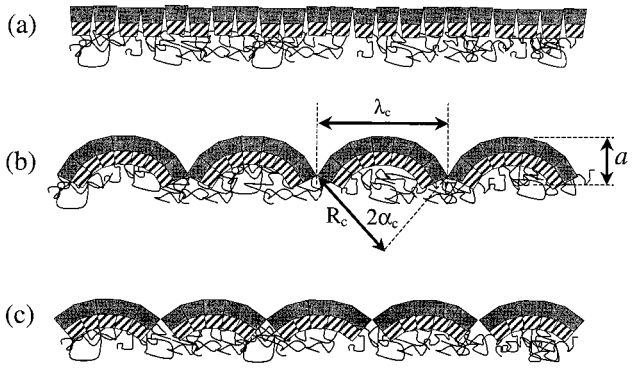

Figure 4. Three potential arrangements of the asymmetric mesogens at the polymer surface: (a) a planar arrangement, (b) polymer surface curved toward the substrate, and (c) a similar curved surface but having a larger defect concentration and lower surface area than (b).

that the domes generally lay on a sloping baseline so that the peak-to-valley height differed on either side of the dome. Although this slope was macroscopically negligible (a maximum slope was ~3°), it can be seen to broaden the final distribution.

It is also useful at this point to determine the mean radius of curvature, R_c, of the dome structures. This can be done directly by assuming the cross-sectional profile of the dome is of the form shown in Figure 4b. In this case, by use of

$$R_c = \frac{(\lambda/2)^2 + a^2}{2a} \tag{1}$$

R_c is calculated to be 43.3 ± 14 nm.

However, this value of R_c is suspect because we have not deconvoluted the effects of the SFM tip radius (~10 nm) from the line scans before extracting a. Therefore, a may be underestimated and R_c overestimated.

A more reliable calculation of R_c can be obtained by a differential geometry analysis of the dome structure. To perform this calculation, individual domes were magnified with imaging software. Their pixel information was then converted into a 2D height matrix. This matrix was transformed into a map of the local mean curvature, H, of the dome using standard finite difference approximations to the following analysis.

The dome surface was described in parametric form as $\mathbf{p}(x,y) = [x,y,z(x,y)]$, where $\mathbf{p}$ is the local position vector of the surface, x and y are the two horizontal axes, and z is a coordinate normal to the average plane of the surface. The local mean curvature is then calculated from[24]

$$H = \frac{EN + GL - 2FM}{2(EG - F^2)} \tag{2}$$

where $E = \mathbf{p}_x \cdot \mathbf{p}_x$, $F = \mathbf{p}_x \cdot \mathbf{p}_y$, $G = \mathbf{p}_y \cdot \mathbf{p}_y$, $L = \mathbf{p}_{xx} \cdot \mathbf{e}$, $M = \mathbf{p}_{xy} \cdot \mathbf{e}$, $N = \mathbf{p}_{yy} \cdot \mathbf{e}$, and $\mathbf{e}$ is the local unit vector normal to the surface. The subscripts on $\mathbf{p}$ denote partial derivatives, for example, $\mathbf{p}_{xy} = \partial^2\mathbf{p}/(\partial x \partial y)$.

Having calculated the curvature matrix for the dome, a radially averaged value about the highest point on the dome was extracted. This procedure was repeated for several domes from all the samples. The corresponding radius of curvature found in this manner was 36.5 ± 1.3 nm within a 5 nm radius of the dome peak. This was considered sufficiently far away from the dome valleys to eliminate any effects of the SFM tip.

In point of fact, back calculating from this result using eq 1 gives a as 1.17 ± 0.13 nm, in agreement (within error) with the line scan analysis. However, in the subsequent discussions we will use the more rigorously obtained value of R_c.

4. Discussion

Because the characteristics of the domes are relatively independent of the block copolymer microstructure and the degree of mesogen attachment, it can be assumed that these structures arise solely from the chemical architecture of the mesogen. The fact that slow cooling through the $S_B \rightarrow I$ transition perfects these structures strongly supports this hypothesis. In general, the macroscopically flat polymer surfaces produce the most enhanced long-range order in the domes. Such flat surfaces arise from either a lamellar block copolymer or from block copolymers with high PS block fractions. In this sense, the nature of the block copolymer domain structure (i.e., whether spherical, cylindrical, or lamellar) does play some role in the organization of the domes. In situ SFM studies of the surface topologies during heating have shown that these structures disappear and reappear during the heating and cooling, respectively, of the block copolymers through the $S_B \rightarrow I$ transition, highlighting the fact that the source of the observed domes arises from the mesogens themselves.[25] However, strong evidence for the origins of the domes comes from SFM studies of thin films of the unattached mesogens. In those studies, films of the unattached mesogens were prepared on silicon by deposition from solution and slow evaporation of the solvent. Because these solutions contained only the mesogenic groups and *none* of the block copolymer, it was hoped to prove that the surface domes we had observed arose solely from the three-armed mesogen. Indeed, in the SFM studies that followed, images virtually identical to that in Figure 2c were obtained.[25]

We believe that the formation of the domes is a direct consequence of the inability of the monodendritic mesogens that form the smectic layer to pack sufficiently well into a planar surface layer (Figure 4a). The $-CF_2-$ portions of each of the three SF groups that form the monodendron occupy a larger volume than the $-CH_2-$ portions.

(24) Nishikawa, Y.; Koga, T.; Jinnai, H.; Hashimoto, T. *Langmuir*, in press.

(25) Sivaniah, E.; Genzer, J.; Fredrickson, G. H.; Kramer, E. J.; Xiang, M.; Li, X.; Ober, C. K.; Magonov, S. In preparation.

Crucially, these three groups are chemically connected to the same carbon atom site. This latter constraint results in an enhanced natural splay of the monodendron molecular architecture over that of the individual SF groups. Therefore, to produce a more uniformly dense surface layer, the mesogens will curve inward toward the substrate producing an architecture shown in Figure 4b.

We can develop a simple thermodynamic model of this surface structure. Let us assume that the surface topology can be approximated by spherical caps of radius R_c, as indicated in cross section in Figure 4b. These spherical caps contact their neighbors to form hexagonal cells in projection. For geometrical convenience, we replace the hexagonal boundary of each cell with a circular boundary of radius $R_c \sin \alpha$, where α is the angle shown in Figure 4b. Our objective is to calculate the total surface energy per unit projected area, E_{total}.

There is a surface tension contribution E_{surf} to E_{total}, given by

$$E_{surf} = \frac{2\sigma(1 - \cos \alpha)}{\sin^2 \alpha} \tag{3}$$

where σ is the surface tension of a fluorinated surface.

This contribution is minimized at low α ($\alpha \Rightarrow 0$ corresponds to a flat surface). However, this situation also leads to a larger number of wedge disclination-like defects in the surface. Each defect contributes a line tension, γ_{def}, to the surface energetics. This is expressed as the defect energy per unit area, E_{defect},

$$E_{defect} = \frac{\gamma_{def}}{R_c \sin \alpha} \tag{4}$$

where γ_{def} is assumed to be independent of α. Under large enough values of γ_{def}, a flat surface is energetically unfavorable. The situation is illustrated graphically by comparing the surfaces of parts b and c of Figure 4 that have an increasing defect concentration and decreasing surface area while R_c remains constant. Thus, there is an optimal geometry (α_c) that lowers the defect energy contribution without increasing the surface area too much. This is obtained by a minimization of E_{total} ($= E_{defect} + E_{surf}$) with respect to α.

E_{total} is minimized when

$$\frac{\gamma_{def}}{\sigma} = 2R_c[\tan \alpha_c - 2 \tan(\alpha_c/2)] \tag{5}$$

which can be expressed at low α_c as

$$\alpha_c \approx \sqrt[3]{\frac{2\gamma_{def}}{R_c\sigma}} \tag{6}$$

Equation 6 qualitatively reflects the situation of our system. At high ratios of γ_{def}/σ, there is a tendency to reduce the defect concentration by increasing α.

It is difficult to predict the system parameter γ_{def} without a better idea of its origins. Rather than speculate, we can extract it using our experimentally derived parameters for R_c, λ, $\sigma = 9 \text{mJ/m}^2$,[22] and α_c [$= \sin^{-1}(\lambda_c/2R_c)$]. In this manner, γ_{def} is found to be $2.9 \pm 0.4 \times 10^{-12}$ N. The line energy, E_{line}, associated with each individual dome, $^1/_2\pi\lambda\gamma_{def}$, is then found to be $(18.1 \pm 2.5)kT$ at the isotropic to smectic transition temperature of 60 °C. This relatively high value of E_{line} indicates the stability of the dome structures in the face of thermal fluctuations and allows for the observed long-range ordering of the domes into an array.

Our model is conceptually similar to one proposed for lipid bilayers by Goetz and Helfrich.[26] Their predictions led to the experimental observation of an "egg carton" phase for complexes of soybean lecithin and cationic polyelectrolytes[27] where the space requirements of two-tailed surfactants necessitate surface buckling.

The surface domes reported in this paper were not observed in the bulk studies of the copolymers because such buckling would hardly perturb the X-ray scattering pattern of what is expected for an ideal lamellar smectic structure. Moreover, the packing constraints found at the surface will be less significant in the bulk. The bulk smectic layers are typically paired layers separated by amorphous regions that contain the isoprene backbone. These smectics may interdigitate or induce local backbone perturbations to pack more efficiently. Such possibilities are not available at the polymer surface. In reaching this model, we have also ignored smectic layer fluctuations.[28] The observed dome structures seem much too regular for such fluctuations to be important.

At the same time, we should discount the creation of superstructures of the type formed by the polymers with attached second and third generation mesogens whose structures were studied in bulk by Hudson et al.[20] These are typically formed from a small number (~20) of mesogens. The resulting superstructures, unsurprisingly, have low radii of curvature (~5 nm) and produce columnar and spherical mesophases. However, the mesogenic structures investigated by Hudson et al. have much larger asymmetries to those used in our first generation monodendron mesogens, and one would expect packing considerations to strongly dominate the behavior in the bulk of the sample. The effect that we observe is due to a more subtle balance of surface forces and packing constraints.

In summary, we have found interesting surface dome structures in monodendron side chain liquid crystalline diblock copolymers that are believed to be a direct consequence of the inability of the semifluorinated side chains to pack efficiently at the polymer surface while still maintaining a planar smectic layer. This structure is relatively independent of the effects of microphase separation of the diblock copolymer, and it is possible to achieve large domains of these hexagonally ordered domes under conditions of lamellar microphase separation. The domes arise from packing constraints due to the asymmetric shape of the conical three-armed mesogen. The modifications made to the polymeric backbone in these studies highlight the flexibility of the liquid crystalline fluoropolymers to simultaneously produce long-range organization at different length scales. The small-scale dome structures we observe have an extraordinary range over which hexagonal ordering is observed and produce a hitherto unreported feature of surface organization.

Acknowledgment. Primary support of this research was provided by the Office of Naval Research, Grant No. N00014-92-J-1246, with added support from the Division of Materials Research, NSF Polymers Program, Grant No. DMR-9803738. This work has made use of MRL central facilities supported by the National Science Foundation under Award No. DMR96-32716.

LA010510M

(26) Goetz, R.; Helfrich, W. *J. Phys. II* **1996**, *6*, 215−223.
(27) Antonietti, M.; Wenzel, A.; Thunemann, A. *Langmuir* **1996**, *12*, 2111−2114.
(28) Holyst, R.; Tweet, D. J.; Sorensen, L. B. *Phys. Rev. Lett.* **1990**, *65*, 2153−2156.